11
Tight-Binding Method for Calculating Raman Spectra

This chapter focuses on the physics involved in calculating Raman spectra, building on the experimental observation of resonance Raman spectra in Chapter 9, and the excitonic nature of the optical transitions discussed in Chapter 10. Besides the strong E_{laser} dependence due to resonance effects, as described in the previous chapters, the Raman intensity also depends on the strength of the matrix elements in the numerator of Eq. (5.20) (see Chapter 5). In the RBM intensity (I_{RBM}) analysis developed in Chapter 9, the matrix elements were assumed to be constant, and this procedure was found to be sufficiently accurate for extracting the resonance transition energies (E_{ii}). However, I_{RBM} strongly depends on the SWNT chirality, that is, on the (n, m) indices, and this dependence requires calculation of the matrix elements. These calculations can only be developed after obtaining the basic electronic structure developed in Chapter 10, and these calculations are not only interesting for explaining the (n, m) dependence of I_{RBM}, but also are needed for developing a fundamental understanding of the physics behind the electron–photon and electron–phonon coupling which strongly influence the observed Raman spectra. Furthermore, the Raman intensity also depends on the resonance window width (γ_r), which broadens the resonance condition while avoiding a singularity in the denominator of Eq. (5.20). The science behind this γ_r parameter can also be calculated and these effects are described in this chapter.

Much of the physics comes from the anisotropic optical absorption in graphene, and these topics will be described here. Although this chapter focuses on both the (n, m) dependence of I_{RBM} and the theoretical description for explaining such a dependence, we only consider the RBM feature as a case study because of its rich behavior and because both experiment and theory are well developed for the RBM feature. The theory discussed here is also important for describing the Raman response for graphene systems in general.

In Section 11.1 we present a few general considerations involved in the calculation of the Raman spectra for graphene and carbon nanotubes, while Section 11.2 summarizes experimental results for the (n, m) dependence of the Raman intensity for carbon nanotubes. Results for a theoretical calculation of the electronic structure are presented in Section 11.3 based on a simple tight-binding calculation. Section 11.4 to Section 11.7 presents an overview of the principles involved in calculating the electron and phonon states and the various pertinent matrix el-

ements and in calculating the Raman intensity. In Section 11.8 we present the parameters for extending the calculations to excitons. In Section 11.9 we combine all the results needed to formulate a calculation of the first-order Raman intensity for carbon nanotubes. In Section 11.10 we introduce the physics of γ_r. We conclude this chapter in Section 11.11 with a brief summary.

11.1
General Considerations for Calculating Raman Spectra

When we calculate the Raman intensity for sp^2 carbons, we need many computational programs in order to calculate physical properties, such as (1) the electronic energy band structure and (2) the phonon dispersion relations. Using the phonon eigenvectors, we can obtain the non-resonant Raman intensity using the so-called bond-polarization theory, in which the polarization induced by the phonon amplitude is proportional to the amplitude of the phonon vibrations [31, 278]. As we discussed in the previous chapters, resonance Raman scattering is essential to describe results for carbon nanotubes, since non-resonance Raman theory cannot account for the interesting phenomena that are observed for sp^2 carbons but can only serve as a basis for symmetry arguments. For calculating the resonance Raman spectra, further physical properties, such as (3) the optical dipole transition matrix elements and (4) the electron–phonon matrix elements are needed. Especially when we consider the general structure of sp^2 carbons (nanotubes, deformed graphene, etc.), the interaction of not only the π electrons, but also the $2s$ and σ electrons should be included. Here, we start with simple tight-binding methods to establish general principles and we use extended tight-binding methods for more detailed calculations, when we consider only π electrons or when we consider a combination of $2s$, σ and π electrons, respectively. Thus we discuss below (1) and (2) within the simple tight-bonding model in Section 11.3 and within the extended tight-binding model in Section 11.4, and then we discuss the more detailed calculations for (3) and (4) within the extended tight-binding model for the remainder of the chapter. Further, in the case of SWNTs, we must consider (5) exciton states, as well as (6) the exciton–photon interaction and (7) the exciton–phonon interaction and their respective matrix elements. Using either electron–phonon or exciton–phonon matrix elements, (8) the resonance window can be determined by evaluating the lifetime of the photoexcited carriers. (9) The phonon life time which is relevant to the Kohn anomaly effect is also calculated by the electron–phonon and exciton–phonon interactions. Within the tight-binding method, computer programs have been developed for calculating the Raman spectra for sp^2 carbons by the authors and their co-workers.

First principles approaches can do the same types of calculations once a set of programs for determining the matrix elements are ready for use. However, it seems that most of the packaged software do not yet contain the programs needed for calculating the electron–photon or electron–phonon matrix elements. Furthermore, it would take a large amount of computational time to obtain the resonance Raman

spectra or the Raman excitation profile if we obtained such results by first principle calculations. The tight-binding method introduced in Section 11.3 is therefore useful to apply to sp^2 carbon materials. In this chapter we show the basic description for topics (1)–(8). For topic (9), we refer the reader to Chapter 8.

This chapter does not describe the calculational methods in detail, but rather overviews the principles of the calculations by introducing the relevant references and the relationship between the calculational programs. This analysis will be useful for the readers in order to understand what is needed for analyzing experimental Raman data and what are the essential points for understanding the observed phenomena.

11.2
The (n, m) Dependence of the RBM Intensity: Experiment

For analyzing the importance of the matrix elements to the Raman cross-section, we compare the RBM intensity for different (n, m) SWNTs satisfying the full resonance condition (i.e., $E_{laser} = E_{ii}$). The RBM spectra from the "super-growth" water-assisted SWNTs have already been extensively analyzed with respect to their resonance energies E_{ii} and their adherence to the $\omega_{RBM} = 227/d_t$ cm^{-1}nm relation, important for the (n, m) assignment (see Chapter 9). These Raman spectra are now ready for an accurate intensity analysis, which is discussed in the present chapter.

High-resolution transmission electron microscopy (HRTEM) imaging was applied to experimentally obtain the d_t distribution of a given super-growth sample, which was then used for RRS characterization [349]. It was here assumed that SWNTs of different chiral angles are equally abundant in the growth process. The relative (n, m) population of the SWNTs must scale as the d_t distribution times $1/d_t$, since the number of different (n, m) species of a given diameter scales linearly with d_t. Also, chiral SWNTs are twice as populous as achiral ones, since both right-handed and left-handed isomers are present in a typical sample. Figure 11.1a shows the intensity calibrated experimental RRS map. The strong features are related to RRS RBM features with E_{ii} transitions.[1] Notice the intensity variation from peak to peak in Figure 11.1a. Especially noticeable is the change in intensity within a given $(2n + m) =$ constant branch. The RBM signal gets stronger when going from larger to smaller chiral angles. Since each spectrum ($S_{(\omega, E_{laser})}$) is the sum of the individual contributions to the observed intensity of all SWNTs, the spectral intensity can be written as:

$$S_{(\omega, E_{laser})} = \sum_{n,m} \left[\text{Pop}_{(n,m)} I^{E_{laser}}_{(n,m)} \frac{\Gamma/2}{(\omega - \omega_{RBM})^2 + (\Gamma/2)^2} \right], \tag{11.1}$$

1) A close inspection of the experimental resonant Raman spectral (RRS) map shows some low-intensity features associated with cross-polarized transitions (E^S_{12}) and RBM overtones. For our purposes, it is safe to ignore cross-polarized and overtone features, since their total contribution to the RRS map is less than 4%.

where $\text{Pop}_{(n,m)}$ is the population of the (n, m) nanotube species, $\Gamma = 3\,\text{cm}^{-1}$ is the experimental average value for the full width at half maximum intensity of the tube's RBM Lorentzian lineshape, ω_{RBM} is the frequency of its RBM and ω is its Raman shift. Each nanotube in the sample contributes to the RBM RRS spectra with one Lorentzian, whose total integrated area ($I_{(n,m)}^{E_{\text{laser}}}$) for the Stokes process at a given excitation laser energy (E_{laser}) is given by:

$$I_{(n,m)}^{E_{\text{laser}}} = \left| \frac{\mathcal{M}}{(E_{\text{laser}} - E_{ii} + i\gamma_r)(E_{\text{laser}} - E_{\text{ph}} - E_{ii} + i\gamma_r)} \right|^2 , \qquad (11.2)$$

where $E_{\text{ph}} = \hbar\omega_{\text{RBM}}$ is the energy of the RBM phonon, E_{ii} is the energy corresponding to the ith excitonic transition, γ_r is a damping factor and $\mathcal{M}$ represents the matrix elements for the Raman scattering by one RBM phonon of the (n, m) nanotube. The values for E_{ii} and ω_{RBM} were determined experimentally (see Chapter 9). $\mathcal{M}$ and γ_r were found by fitting the experimental RBM RRS map with Eq. (11.1) using the functions:

$$\mathcal{M} = \left[\mathcal{M}_{\text{A}} + \frac{\mathcal{M}_{\text{B}}}{d_{\text{t}}} + \frac{\mathcal{M}_{\text{C}} \cos(3\theta)}{d_{\text{t}}^2} \right]^2$$

$$\gamma_r = \gamma_{\text{A}} + \frac{\gamma_{\text{B}}}{d_{\text{t}}} + \frac{\gamma_{\text{C}} \cos(3\theta)}{d_{\text{t}}^2} , \qquad (11.3)$$

where $\mathcal{M}_i$ and γ_i ($i = $ A, B, C) are adjustable parameters that also account for their dependence on (n, m) or equivalently on (d_{t}, θ). The best values for $\mathcal{M}_i$ and γ_i, considering the excitonic transitions E_{22}^S and the lower branch of E_{11}^M are listed in Table 11.1 for d_{t} in nm, γ_r in meV and $\mathcal{M}$ in arbitrary units since the Raman intensity is usually given by arbitrary units.

Using Eqs. (11.1)–(11.3) the values in Eq. (11.1), we obtain the modeled RRS map shown in Figure 11.1b, which accounts for the experimentally observed results shown in Figure 11.1a very well. To understand the (n, m) dependence of
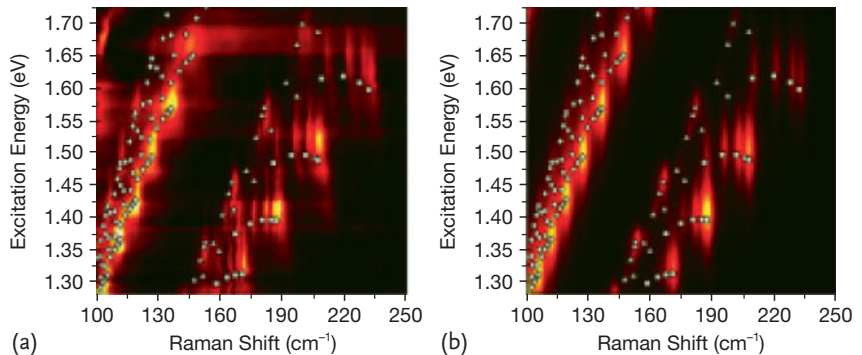

Figure 11.1 (a) Experimental RRS map for the radial breathing mode feature. The intensity calibration was made by measuring a standard tylenol sample. (b) Modeled map obtained by using Eq. (11.1) and the same laser excitation energies range as in (a) [349].

Table 11.1 Fitted parameters $\mathcal{M}_i$ and γ_i for metallic, semiconductor type 1 and type 2 tubes. These parameters are to be used in Eq. (11.3) with d_t in nm, yielding $\mathcal{M}$ in arbitrary units and γ_i in meV.

Type	$\mathcal{M}_A$	$\mathcal{M}_B$	$\mathcal{M}_C$	γ_A	γ_B	γ_C
M	1.68	0.52	5.54	23.03	28.84	1.03
S_1	−19.62	29.35	4.23	−3.45	65.10	7.22
S_2	−1.83	3.72	1.61	−10.12	42.56	−6.84

both $\mathcal{M}$ and γ_r, described by Eq. (11.3), the next sections address their (n, m) dependence theoretically. Before discussing the direct calculation of the matrix elements and resonance window widths, we first describe the calculations for electron and phonon states.

11.3
Simple Tight-Binding Calculation for the Electronic Structure

In this section first, we review the tight-binding method for the electronic energy bands for sp^2 carbons and then apply this method to the electronic structure of graphite. In a perfectly periodic system, any wavefunction for an energy band satisfies the Bloch theorem [118]. A Bloch function is a basis wavefunction which satisfies the Bloch theorem. Typical examples of Bloch functions are plane wave and tight-binding wavefunctions. A large (complete) set of the plane wave functions can express the energy band precisely by solving the Hamiltonian as a function of the wave vector k. The computational accuracy of the plane wave expansion is determined by how many plane waves are adopted in the computation for a given unit cell which is specified by a cut-off energy. The plane wave expansion for energy band calculations is mainly used for first principle calculations which does not explicitly specify the atom species contained in the structure of the solid or of the molecule. As far as we consider only the sp^2 carbon system, the tight-binding method is useful for understanding the physics and for saving computational time.

As described in Section 2.2, the tight-binding wavefunction $\Psi_j(k)$, where j denotes the energy band index, is given by a linear combination of a small number of tight-binding Bloch wave functions $\Phi_{j'}$

$$\Psi_j(k, r) = \sum_{j'=1}^{N} C_{jj'}(k)\Phi_{j'}(k, r), \quad (j = 1, \cdots, N),$$ (11.4)

where $C_{jj'}(k)$ are coefficients to be determined and N is the number of atomic orbitals in the unit cell. From an atomic orbital φ_j in the unit cell, we can construct the tight-binding Bloch function Φ_j as

$$\Phi_j(k, r) = \frac{1}{\sqrt{N_u}} \sum_{R}^{N_u} e^{ik \cdot R} \varphi_j(r - R), \quad (j = 1, \cdots, N),$$ (11.5)

where the summation takes place over N_u lattice vectors $\boldsymbol{R}$ in the crystals. When we define the Hamiltonian and the overlap matrices, $\mathcal{H}_{jj'}(\boldsymbol{k})$ and $\mathcal{S}_{jj'}(\boldsymbol{k})$, respectively,

$$\mathcal{H}_{jj'}(\boldsymbol{k}) = \langle \Phi_j | \mathcal{H} | \Phi_{j'} \rangle \,, \quad \mathcal{S}_{jj'}(\boldsymbol{k}) = \langle \Phi_j | \Phi_{j'} \rangle \,, \quad (j, j' = 1, \cdots, N) \,. \tag{11.6}$$

The Schrödinger equation is given in terms of the simultaneous equations

$$\sum_{j'=1}^{N} \mathcal{H}_{jj'}(\boldsymbol{k}) C_{ij'} = E_i(\boldsymbol{k}) \sum_{j'=1}^{N} \mathcal{S}_{jj'}(\boldsymbol{k}) C_{ij'} \quad (i = 1, \cdots, N) \,. \tag{11.7}$$

Defining a column vector by

$$\boldsymbol{C}_i = \begin{pmatrix} C_{i1} \\ \vdots \\ C_{iN} \end{pmatrix} \,. \tag{11.8}$$

Then Eq. (11.7) is expressed by

$$\mathcal{H} \boldsymbol{C}_i = E_i(\boldsymbol{k}) \mathcal{S} \boldsymbol{C}_i \,. \tag{11.9}$$

By using a numerical calculation for the diagonalization of a given $\mathcal{H}$ and $\mathcal{S}$ for each $\boldsymbol{k}$, we get the energy eigenvalues $E_i(\boldsymbol{k})$ and eigenfunctions $\boldsymbol{C}_i(\boldsymbol{k})$.[2]

The ij matrix element of $\mathcal{H}$ is expressed by

$$\begin{aligned} \mathcal{H}_{ij}(\boldsymbol{k}) &= \frac{1}{N_u} \sum_{R,R'} e^{ik(R-R')} \langle \varphi_i(r - R') | \mathcal{H} | \varphi_j(r - R) \rangle \\ &= \sum_{\Delta R} e^{ik(\Delta R)} \langle \varphi_i(r - \Delta R) | \mathcal{H} | \varphi_j(r) \rangle \,, \end{aligned} \tag{11.10}$$

where $\Delta R \equiv R - R'$ is the distance between carbon atoms in graphite as illustrated in Figure 11.2 and in the second line of Eq. (11.10), we use the fact that $\langle \varphi_i(r - R') | \mathcal{H} | \varphi_j(r - R) \rangle$ only depends on ΔR. Similarly, $\mathcal{S}$ is given by:

$$\mathcal{S}_{ij}(\boldsymbol{k}) = \sum_{\Delta R} e^{ik(\Delta R)} \langle \varphi_i(r - \Delta R) | \varphi_j(r) \rangle \,. \tag{11.11}$$

The tight-binding parameters for $\mathcal{H}$ and $\mathcal{S}$ in Eqs. (11.10) and (11.11) are defined, respectively, by $\langle \varphi_i(r - \Delta R) | \mathcal{H} | \varphi_j(r) \rangle$ and $\langle \varphi_i(r - \Delta R) | \varphi_j(r) \rangle$ for some nearest neighbor ΔR from knowledge of the $\varphi_j(r)$ atomic orbitals. The tight-binding parameters are given so as to reproduce the experimental atomic energy dispersion data obtained by angle-resolved photoemission spectroscopy (ARPES) or first principles calculations. A typical parameter set (TBP) is listed in Table 11.2 for the 3NN (3rd nearest neighbor tight-binding parameters coupling three graphene layers) as shown in Figure 11.2 [350].

---

2) We use the LAPAC library (zhegv) for the diagonalization of a Hermitian matrix $\mathcal{A}$ in terms of a positive definite Hermitian matrix $\mathcal{B}$, that obeys $\mathcal{A}\boldsymbol{C} = E\mathcal{B}\boldsymbol{C}$. The output of the "zhegv" subprogram is $E_i(\boldsymbol{k})$ and $\boldsymbol{C}_i(\boldsymbol{k})$.

Table 11.2 Third nearest neighbor tight-binding (3NN TB) parameters for few-layer graphene and graphite. All values are in electron volt except for the parameters s_0–s_2 which are dimensionless. The parameters coming from fits to LDA and GW calculations are shown. The 3NN Hamiltonian is valid over the whole two (three)-dimensional Brillouin zone (BZ) of graphite (graphene layers) [350].

TBP	3NN TB-GW[a]	3NN TB-LDA[a]	EXP[b]	3NN TB-LDA[c]	ΔR, pair[d]
γ_0^1	−3.4416	−3.0121	−5.13	−2.79	$a/\sqrt{3}$, AB
γ_0^2	−0.7544	−0.6346	1.70	−0.68	a, AA and BB
γ_0^3	−0.4246	−0.3628	−0.418	−0.30	$2a/\sqrt{3}$, AB
s_0	0.2671	0.2499	−0.148	0.30	$a/\sqrt{3}$, AB
s_1	0.0494	0.0390	−0.0948	0.046	a, AA and BB
s_2	0.0345	0.0322	0.0743	0.039	$2a/\sqrt{3}$, AB
γ_1	0.3513	0.3077	–	–	c, AA
γ_2	−0.0105	−0.0077	–	–	$2c$, BB
γ_3	0.2973	0.2583	–	–	$(a/\sqrt{3}, c)$, BB
γ_4	0.1954	0.1735	–	–	$(a/\sqrt{3}, c)$, AA
γ_5	0.0187	0.0147	–	–	$2c$, AA
E_0[e]	−2.2624	−1.9037	–	−2.03	
Δ[f]	0.0540[g]	0.0214	–	–	

a fits to LDA and GW calculations[350]
b fit to ARPES experiments by Bostwick *et al.* [351]
c fit to LDA calculations by Reich *et al.* [115]
d in-plane and out-of-plane distances between a pair of A and B atoms.
e the energy position of π orbitals relative to the vacuum level.
f difference of the diagonal term between A and B atoms for multi-layer graphene.
g the impurity doping level due to unintended dopants is adjusted in order to reproduce the experimental value of Δ in graphite.

As seen in Table 11.2, many research groups have so far obtained a set of tight-binding parameters for graphite, carbon nanotubes and graphene. In Figure 11.2,
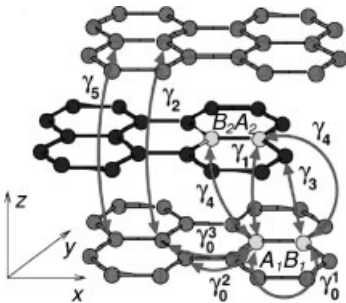

Figure 11.2 Identification of the various Slonczewski–Weiss parameters which describe the tight-binding parameters for a pair of carbon atoms separated by a distance ΔR in graphite [350].

we show a definition of the tight-binding parameters for the Hamiltonian in Eq. (11.10) for pairs of carbon atoms separated by their corresponding distances ΔR [350] in Table 11.2. The notation γ_i for the tight-binding parameters follows that of Slonczewski and Weiss [97] in which γ_0^j, ($j = 1, 2, 3$) denotes the in-plane parameters with the jth nearest neighbors up to the 3rd nearest neighbor (3NN). As far as we consider transport properties near the K point of the first Brillouin zone, the in-plane nearest neighbor parameter γ_0^1 is sufficient. However, when we consider optical transition phenomena around the K point, the further neighbor terms (see Figure 11.2) γ_0^2 and γ_0^3 are also necessary [115]. The parameters γ_1, γ_3, and γ_4 denote interactions between carbon atoms in adjacent layers (see Figure 11.2), while the parameters γ_2 and γ_5 couple carbon atoms between the second nearest neighbor layers. The parameters γ_3 and γ_4 introduce a $\boldsymbol{k}$-dependent interlayer interaction and γ_2 determines a small energy dispersion along the KH direction in the three-dimensional Brillouin zone which gives rise to an electron and a hole carrier pocket, such as is observed for the semimetal graphite.

As for the overlap tight-binding parameters, s_0, s_1, and s_2, in Eq. (11.11) we only consider the in-plane parameters. These parameters are essential for describing the asymmetry between the valence and conduction energy bands of graphite relative to the Fermi energy. The values of these parameters for graphite provide a larger energy band width for the conduction band than that for the valence band consistent with detailed optical and transport measurements in graphite [16].

11.4
Extended Tight-Binding Calculation for Electronic Structures

The simple tight-binding parameters obtained in Section 11.3 are for π orbitals for graphite or few layer graphene. When we consider SWNTs with different diameters, we must consider new tight-binding parameters for each SWNT diameter since the curvature of the cylindrical tube surface mixes π orbitals with σ orbitals (or equivalently ($2p_x$ and $2p_y$) and $2s$ orbitals). Furthermore, when we consider an optimization of the bond length or of the geometrical structure, we need to calculate tight-binding parameters as a function of the various C–C bonds.

The extended tight-binding (ETB) calculation is a tight-binding calculation for π, σ, and $2s$ orbitals, in which the tight-binding parameters for a pair of orbitals and for a particular ΔR are given as a function of the pertinent C–C bond lengths. The functions of the tight-binding parameters are given by first principles calculations for several sp^2 molecules or solids so as to reproduce the optimized C–C bond lengths and bond angles of many sp^2 materials. For carbon systems, the tight-binding parameters as a function of the C–C bond lengths have been calculated by Porezag [263], and this calculation is adopted for optimized calculations of SWNTs with diameters smaller than 1 nm [182]. The ETB calculation of smaller

diameter SWNTs reproduces well the observed family pattern[3] of the optical transition energies. The observed family pattern is considered to be due to a curvature effect.

In quantum chemistry calculations, great effort has been put into calculating these tight-binding parameters as a function of the bond lengths for many different elements of the periodic table using so-called semi-empirical methods. MNDO, MINDO, AM3, and PM5 are names of the parameter sets for popular semi-empirical methods, which are used in many chemistry molecular level calculations packages such as MOPAC and Gaussian, etc. An advantage of the ETB or the semi-empirical method is that the calculation of the optimized structure is easy and thus the speed of the calculation is fast. Thus even when first principle calculations are employed, semi-empirical calculations are in fact used for a preliminary determination of the initial values.

11.5
Tight-Binding Calculation for Phonons

As described in Section 3.2, the phonon energy dispersion can be calculated by a set of springs which connect some nearest neighbor atoms and these theoretical calculations are fitted to experimentally derived phonon dispersion relations, such as are obtained from neutron or X-ray inelastic scattering measurements. The equations of motion used to describe such vibrations are given by:

$$M_i \ddot{\boldsymbol{u}}_i = \sum_j K^{(ij)}(\boldsymbol{u}_j - \boldsymbol{u}_i) , \quad (i = 1, \dots, N) , \tag{11.12}$$

where M_i is the mass of the ith atom and $K^{(ij)}$ represents the 3×3 force constant tensor. The summation on j is taken over jth nearest neighbor atoms so as to reproduce the phonon energy dispersion relation. When we use the Bloch theorem for deriving an expression for $\boldsymbol{u}_i$ to obtain the amplitude of the vibration with the phonon wave vector $\boldsymbol{q}$ and frequency ω, we get,

$$\boldsymbol{u}_q^{(i)} = \frac{1}{\sqrt{N_u}} \sum_{R_i} e^{i(q \cdot R_i - \omega t)} \boldsymbol{u}_i , \tag{11.13}$$

where the sum is taken over all $N_u \boldsymbol{R}_i$ vectors in the crystal for the ith atoms in the unit cell. The equation for $\boldsymbol{u}_q^{(i)}$ ($i = 1, \dots, N$), where N is the number of atoms in the unit cell, is given by [31]:

$$\left[\sum_j K^{(ij)} - M_i \omega^2(q) I \right] \boldsymbol{u}_q^{(i)} - \sum_j K^{(ij)} e^{iq \cdot \Delta R_{ij}} \boldsymbol{u}_q^{(j)} = 0 , \tag{11.14}$$

3) Optical transition energies E_{ii} of an (n, m) SWNT with $2n + m =$ constant show a similar energy to one another. When we plot E_{ii} as a function of the diameter, we can see a pattern for SWNTs with $2n + m =$ constant. The observed pattern is called the family pattern and the values of $2n + m$ are called the family number. (See Section 10.4.4.)

where I is a 3×3 unit matrix and $\Delta R_{ij} = R_i - R_j$ is the relative coordinate of the ith atom with respect to the jth atom. The simultaneous equations implied by Eq. (11.14) with $3N$ unknown variables $u_q \equiv (u_q^{(1)}, u_q^{(2)}, \cdots, u_q^{(N)})^t$, for a given k vector, can be solved by diagonalization of the $3N \times 3N$ matrix in brackets, which we call the dynamical matrix, and here we look for a non-trivial solution for $u_q \neq 0$ for each q point.

11.5.1
Bond Polarization Theory for the Raman Spectra

Once the phonon eigenvectors u_k are obtained, we can estimate the Raman intensity by use of bond polarization theory. The Raman intensity $I_{\eta'\eta}(\omega)$ for $\mathcal{N}$ atoms in the unit cell is then calculated by the empirical bond polarizability model [352, 353]

$$I_{\eta'\eta}(\omega) \propto \omega_L \omega_S^3 \sum_{f=1}^{3N} \frac{\langle n(\omega_f) \rangle + 1}{\omega_f} \left| \sum_{\alpha\beta} \eta'_\alpha \eta_\beta P_{\alpha\beta,f} \right|^2 \delta(\omega - \omega_f), \quad (11.15)$$

where ω_L, ω_S, and ω_f are, respectively, the frequencies for the incident and scattered light[4] and the fth phonon frequency at the Γ point, and η and η' are the corresponding unit vectors for the incident and scattered light polarization, respectively. Here $\langle n(\omega_f) \rangle = 1/(\exp(\hbar\omega_f/k_B T) - 1)$ is the Boltzmann occupation number for the phonon, while $P_{\alpha\beta,f}$ is the derivative of the electronic polarization tensor with respect to a change in the C–C bond, in which α and β denote the Cartesian components. Bond polarization theory can be applied to graphite, graphene and nanotubes.

The polarization tensor is modified by the phonon vibration in which the electronic polarization $P_{\alpha\beta,f}$ is proportional to the amplitude of the phonon vibration. After some calculation, we get [31]

$$P_{\alpha\beta,f} = -\sum_{\ell B} \left[\frac{R_0(\ell, B) \cdot \chi(\ell|f)}{R_0(\ell, B)} \times \left\{ \left(\frac{\alpha'_\parallel(B) + 2\alpha'_\perp(B)}{3} \right) \delta_{\alpha\beta} \right. \right.$$

$$+ \left(\alpha'_\parallel(B) - \alpha'_\perp(B) \right) \left(\frac{R_{0\alpha}(\ell, B) R_{0\beta}(\ell, B)}{R_0(\ell, B)^2} - \frac{1}{3}\delta_{\alpha\beta} \right) \right\}$$

$$+ \left(\frac{\alpha_\parallel(B) - \alpha_\perp(B)}{R_0(\ell, B)} \right) \left\{ \frac{R_{0\alpha}(\ell, B)\chi_\beta(\ell|f) - R_{0\beta}(\ell, B)\chi_\alpha(\ell|f)}{R_0(\ell, B)} \right.$$

$$\left. \left. - \frac{R_0(\ell, B) \cdot \chi(\ell|f)}{R_0(\ell, B)} \times \frac{2 R_{0\alpha}(\ell, B) R_{0\beta}(\ell, B)}{R_0(\ell, B)^2} \right\} \right], \quad (11.16)$$

where $\chi(\ell|f)$ denotes the unit vectors of the fth normal modes of the ℓth atom, B denotes a bond which is connected to the ℓth atom in the unit cell, and $\mathbf{R}(\ell, \mathbf{B})$ is

---

4) Since $\omega_L \sim \omega_S$ for the incident and scattered light, we can say that the intensity is proportional to ω_S^4 which is discussed in Section 5.5.

Table 11.3 Bond lengths and Raman polarizability parameters for single-wall carbon nanotubes and for various carbon-related molecules.

Molecule	Bond lengths [Å]	$\alpha_\| + 2\alpha_\perp$ [Å³]	$\alpha_\| - \alpha_\perp$ [Å³]	$\alpha'_\| + 2\alpha'_\perp$ [Å²]	$\alpha'_\| - \alpha'_\perp$ [Å²]
CH_4[a]	C–H (1.09)	1.944			
C_2H_6[a]	C–C (1.50)	2.016	1.28	3.13	2.31
C_2H_4[a]	C=C (1.32)	4.890	1.65	6.50	2.60
C_{60}[b]	C–C (1.46)		1.28	2.30 ± 0.01	2.30 ± 0.30
	C=C (1.40)		0.32 ± 0.09	7.55 ± 0.40	2.60 ± 0.36
C_{60}[a]	C–C (1.46)		1.28 ± 0.20	1.28 ± 0.30	1.35 ± 0.20
	C=C (1.40)		0.00 ± 0.20	5.40 ± 0.70	4.50 ± 0.50
SWNT[c]	C=C (1.42)		0.07	5.96	5.47
SWNT[d]	C=C (1.42)		0.04	4.7	4.0

a S. Guha *et al.* [352].
b D. W. Snoke *et al.* [354].
c A. M. Rao *et al.* (unpublished data which is used in their work [136]).
d R. Saito *et al.* [278].

the corresponding vector from the ℓth atom to the neighboring atom ℓ' specified by B. Here $\alpha'_\|(B)$ and $\alpha'_\perp(B)$ are the radial derivatives of $\alpha_\|(B)$ and $\alpha_\perp(B)$, that is

$$\alpha'_\|(B) \equiv \frac{\partial \alpha_\|(B)}{\partial R(\ell, B)}, \quad \text{and} \quad \alpha'_\perp(B) \equiv \frac{\partial \alpha_\perp(B)}{\partial R(\ell, B)}, \tag{11.17}$$

respectively. The values of $\alpha_\|(B)$, $\alpha_\perp(B)$, $\alpha'_\|(B)$ and $\alpha'_\perp(B)$ have been reported by some groups empirically as a function of the bond lengths between two carbon atoms or between carbon-hydrogen atoms, and these values are listed for carbon nanotubes in Table 11.3.

Thus once we obtain the phonon eigenvectors, the Raman intensity can be calculated by using the empirical values for the appropriate bond polarizability parameters (see Table 11.3). The Raman intensity thus obtained is for a non-resonance Raman signal. However, one can use these results to specify qualitatively which Raman-active modes give a relatively strong signal or how the Raman signal changes by changing the polarization direction of the light.

11.5.2
Non-Linear Fitting of Force Constant Sets

The force constant matrix is obtained by minimizing the least square values of $\mathcal{F}$,

$$\mathcal{F} \equiv \sum_k \frac{\left(f_k^{\text{obs.}} - f_k^{\text{cal.}}\right)^2}{\sigma_k^2}, \tag{11.18}$$

Table 11.4 Force constant parameters of graphite in units of 10^4 dyn/cm. Here the subscripts r, ti, and to refer to radial, transverse in-plane, and transverse out-of-plane force constants, respectively.

Fitted force constants	Jishi *et al.* neutron [123]	Grüneis *et al.* theory[133]	Dubay *et al.* *ab initio* [124]	Maultzsch *et al.* X-ray [129]	Zimmerman *et al.* theory [355]
$\phi_r^{(1)} =$	36.50	40.37	44.58	39.28	41.80
$\phi_r^{(2)} =$	8.80	2.76	7.31	6.34	7.60
$\phi_r^{(3)} =$	3.00	0.05	−5.70	−6.14	−0.15
$\phi_r^{(4)} =$	−1.92	1.31	1.82	2.53	−0.69
$\phi_{ti}^{(1)} =$	24.50	25.18	11.68	11.36	15.20
$\phi_{ti}^{(2)} =$	−3.23	2.22	−3.74	−3.18	−4.35
$\phi_{ti}^{(3)} =$	−5.25	−8.99	6.67	9.27	3.39
$\phi_{ti}^{(4)} =$	2.29	0.22	0.52	−0.40	−0.19
$\phi_{to}^{(1)} =$	9.82	9.40	10.00	10.18	10.20
$\phi_{to}^{(2)} =$	−0.40	−0.08	−0.83	−0.36	−1.08
$\phi_{to}^{(3)} =$	0.15	−0.06	0.51	−0.46	1.00
$\phi_{to}^{(4)} =$	−0.58	−0.63	−0.54	−0.44	−0.55

where $f_k^{obs.}$, $f_k^{cal.}$, and σ_k denote, respectively, the observed phonon frequency, the calculate phonon frequency and the error bar (or the weight) of the observed phonon frequency at the k point. The force constant parameter sets are determined by a non-linear fitting procedure so as to minimize $\mathcal{F}$. The fitting procedure is not so easy when using a large number of the force constants, since there are many local minima of $\mathcal{F}$ in the parameter space. In order to avoid this problem by getting out of a local minimum to a global minimum, some computer techniques are required.[5]

In Table 11.4, we list the force constants labeled by ϕ for the earliest result of a fit to inelastic neutron scattering data by Jishi *et al.* [123], theoretical data by Grüneis *et al.* [133] and by Dubay *et al.* [124], inelastic X-ray scattering data by Maultzsch *et al.* [129] and theoretical work by Zimmerman *et al.* [355]. The force constant matrix tensor K_{ij} for a given C–C bond is calculated by rotating the diagonal matrix for a pair of two carbon atoms on the x axis whose diagonal elements are ϕ_r, ϕ_{ti} and ϕ_{to}, which are clearly defined relative to the C–C bond direction [31].

An important quantity that we should consider is the so-called *force constant sum rules* [356] which are used to impose the condition $\omega = 0$ for acoustic phonons. Since all forces K_{ij} are internal forces between the ith and jth atoms, there should be no total force on the system. Otherwise, the materials would automatically move or rotate around their center of mass. Since the sum of internal forces vanishes, the

---

5) The non-linear fitting procedure depends on the systems considered and there is not a unique way to get to the global minimum. A recommended way to approximate the global minimum is to increase the parameters one by one using the optimized values of the previous calculation as the initial values when adding one additional parameter.

translational invariance is automatically satisfied. However, the rotation around the center of the mass is not always satisfied by a finite number of force constant sets. When we consider the rotation around the ith atom, if the following condition for the jth tangential force constants $\phi_{\mathrm{ti}}^{(j)}$ and $\phi_{\mathrm{to}}^{(j)}$ [355] is satisfied

$$\sum_j^n n_j \phi_t^{(j)} \Delta R_{ij}^2 = 0 , \quad (t = ti \quad \text{or} \quad to) , \tag{11.19}$$

then the corresponding increase of the potential energy around the ith atom will disappear. Here n_j and ΔR_{ij} are, respectively the number and the distance of the jth atom from the original ith atom. In the case of graphene, there are four tangential phonon modes, that is, iTA, iTO, oTA, and oTO modes, for which Eq. (11.19) must be satisfied for $\phi_{\mathrm{ti}}^{(j)}$ and $\phi_{\mathrm{to}}^{(j)}$. For a force constant set for radial motion, since the force and ΔR_{ij} are parallel to each other, no torques occur. This force constant sum rule is essential for finding the zero values at the Γ point in the Brillouin zone for the acoustic phonon branches. At other k points, the phonon eigenvalues should never be negative (or imaginary), since the dynamical matrix is a positive Hermitian matrix.

The force constant rules given by (Eq. (11.19)) can be used in non-linear fitting procedures (such as for a Lagrange multiplier method) or we can simply define the outermost force constant parameter so as to satisfy Eq. (11.19).

11.6
Calculation of the Electron–Photon Matrix Element

The electron–photon matrix element is calculated in terms of an electron dipole-transition of π electrons. The optical dipole transition from a π (2p) state to an unoccupied π state of an electron within an atom is forbidden. Thus the optical transition between a π and a π^* energy band is possible for the nearest neighbor electron–photon matrix elements as shown below.

The perturbation Hamiltonian of the dipole transition is given by:

$$H_{\mathrm{opt}} = \frac{ie\hbar}{m} A(t) \cdot \nabla , \tag{11.20}$$

where A is the vector potential. Here we adopt the Coulomb gauge $\nabla \cdot A(t) = 0$. In this case, the electric field of the light is given by $E = i\omega A$. Hereafter we consider only a linear polarization of the light and thus the vector potential A is given by:

$$A = \frac{-i}{\omega} \sqrt{\frac{I}{c\epsilon_0}} \exp(\pm i\omega t) P , \tag{11.21}$$

where P is the unit vector (polarization vector) which specifies the direction of E, while I is the intensity of the light in W/m^2 and ϵ_0 is the dielectric constant

for vacuum using SI units. The "$\pm$" sign corresponds to the emission ("+") or absorption ("−") of a photon with frequency ω.

The matrix element for optical transitions from an initial state ι at $\boldsymbol{k} = \boldsymbol{k}_\iota$, denoted by $\Psi^\iota(\boldsymbol{k}_\iota)$ to a final state f denoted by $\Psi^f(\boldsymbol{k}_f)$ at $\boldsymbol{k} = \boldsymbol{k}_f$, is defined by

$$M_{\mathrm{opt}}^{f\iota}(\boldsymbol{k}_f, \boldsymbol{k}_\iota) = \left\langle \Psi^f(\boldsymbol{k}_f) \right| H_{\mathrm{opt}} \left| \Psi^\iota(\boldsymbol{k}_\iota) \right\rangle \; . \tag{11.22}$$

The electron–photon matrix element in Eq. (11.22) is calculated by

$$M_{\mathrm{opt}}^{f\iota}(\boldsymbol{k}_f, \boldsymbol{k}_\iota) = \frac{e\hbar}{m\omega_\rho}\sqrt{\frac{I_\rho}{c\epsilon_0}}\, e^{i(\omega_f - \omega_\iota \pm \omega)t}\, \boldsymbol{D}^{f\iota}(\boldsymbol{k}_f, \boldsymbol{k}_\iota) \cdot \boldsymbol{P} \; , \tag{11.23}$$

where the electric dipole vector between initial states ι and final states f denoted by $\boldsymbol{D}^{f\iota}(\boldsymbol{k}_f, \boldsymbol{k}_\iota)$ is defined by

$$\boldsymbol{D}^{f\iota}(\boldsymbol{k}_f, \boldsymbol{k}_\iota) = \langle \Psi^f(\boldsymbol{k}_f)|\nabla|\Psi^\iota(\boldsymbol{k}_\iota)\rangle \; . \tag{11.24}$$

For a given polarization, $\boldsymbol{P}$, when $\boldsymbol{D}$ is parallel to $\boldsymbol{P}$, the optical absorption (or stimulated emission) is the largest, while when $\boldsymbol{D}$ is perpendicular to $\boldsymbol{P}$, the optical absorption is absent.

11.6.1
Electric Dipole Vector for Graphene

Let us now consider the electric dipole vector for graphene [220]. The wavefunction in Eq. (11.4) with $n = 2$ is given by $\Psi(\boldsymbol{k}) = C_A \Phi_A(\boldsymbol{k}, \boldsymbol{r}) + C_B \Phi_B(\boldsymbol{k}, \boldsymbol{r})$, in which Φ is the Bloch wavefunction for $2p_z$ atomic orbitals for the A and B sites of graphene. Then the electric dipole vector $\boldsymbol{D}^{f\iota}(\boldsymbol{k}_f, \boldsymbol{k}_\iota)$ for graphene is given by:

$$\begin{aligned} \boldsymbol{D}^{f\iota}(\boldsymbol{k}_f, \boldsymbol{k}_\iota) = {}& C_B^{f*}(\boldsymbol{k}_f) C_A^\iota(\boldsymbol{k}_\iota)\langle \Phi_B(\boldsymbol{k}_f, \boldsymbol{r})|\nabla|\Phi_A(\boldsymbol{k}_\iota, \boldsymbol{r})\rangle \\ & + C_A^{f*}(\boldsymbol{k}_f) C_B^\iota(\boldsymbol{k}_\iota)\langle \Phi_A(\boldsymbol{k}_f, \boldsymbol{r})|\nabla|\Phi_B(\boldsymbol{k}_\iota, \boldsymbol{r})\rangle \; . \end{aligned} \tag{11.25}$$

Since the $2p_z$ orbital and the $\partial/\partial z$ component of ∇ all have odd symmetry with respect to the z mirror plane, the z component of $\boldsymbol{D}$ becomes zero. When we expand the Bloch function into an atomic orbital, the leading term of $\langle \Phi_A(\boldsymbol{k}_f, \boldsymbol{r})|\nabla|\Phi_B(\boldsymbol{k}_\iota, \boldsymbol{r})\rangle$ is the atomic matrix element between nearest neighbor atoms

$$m_{\mathrm{opt}} = \langle \phi(\boldsymbol{r} - \boldsymbol{R}_{\mathrm{nn}})|\frac{\partial}{\partial x}|\phi(\boldsymbol{r})\rangle \; , \tag{11.26}$$

where $\boldsymbol{R}_{\mathrm{nn}}$ is the vector between nearest neighbor atoms along the x axis.

When we use approximate coefficients C_A and C_B for a $\boldsymbol{k}$ point around $\boldsymbol{K} = (0, -4\pi/(3a))$,

$$C_A^c(\boldsymbol{K} + \boldsymbol{k}) = \frac{1}{\sqrt{2}} , \quad C_B^c(\boldsymbol{K} + \boldsymbol{k}) = \frac{-k_y + i k_x}{\sqrt{2}k} ,$$

$$C_A^v(\boldsymbol{K} + \boldsymbol{k}) = \frac{1}{\sqrt{2}} , \quad C_B^v(\boldsymbol{K} + \boldsymbol{k}) = \frac{k_y - i k_x}{\sqrt{2}k} , \tag{11.27}$$

where c and v denote the conduction and valence energy bands, respectively. The electric dipole vector is then given by:

$$\boldsymbol{D}^{cv}(\boldsymbol{K} + \boldsymbol{k}) = \frac{3m_{opt}}{2k}(k_y, -k_x, 0) . \tag{11.28}$$

In Figure 11.3a we plot the normalized directions of $\boldsymbol{D}^{cv}(\boldsymbol{k})$ as arrows over the 2D Brillouin zone of graphene. Around the K points, the arrows show a vortex behavior. Note also that the rotational directions of $\boldsymbol{D}^{cv}(\boldsymbol{k})$ around the K and K' points are opposite to each other in Figure 11.3.

In Figure 11.3b we plot the values of the oscillator strength $O(\boldsymbol{k})$ in units of m_{opt} (see Eq. (11.26)) on a contour plot. Here $O^{cv}(\boldsymbol{k})$ is defined by

$$O^{cv}(\boldsymbol{k}) = \sqrt{\boldsymbol{D}^{cv*}(\boldsymbol{k}) \cdot \boldsymbol{D}^{cv}(\boldsymbol{k})} . \tag{11.29}$$

From Figure 11.3b it is clear that the oscillator strength $O^{cv}(\boldsymbol{k})$ has a maximum at the M points and a minimum at the Γ point in the Brillouin zone. The $\boldsymbol{k}$ dependent $O^{cv}(\boldsymbol{k})$ will be relevant to the type-dependent photoluminescence intensity of a single-wall carbon nanotube [357] though we need to consider the electric dipole vector for each carbon nanotube individually in terms of its diameter and chiral angle [220, 358, 359].

For getting the optical absorption intensity, we take the inner dot product $\boldsymbol{D}^{cv}(\boldsymbol{k}) \cdot \boldsymbol{P}$ up to terms linear in k_x and k_y for a given polarization vector $\boldsymbol{P} = (p_x, p_y, p_z)$

$$\boldsymbol{P} \cdot \langle \Psi^c(\boldsymbol{k}) | \nabla | \Psi^v(\boldsymbol{k}) \rangle = \pm \frac{3m_{opt}}{2k}(p_y k_x - p_x k_y) . \tag{11.30}$$

(a)　　　　　　　　　　(b)
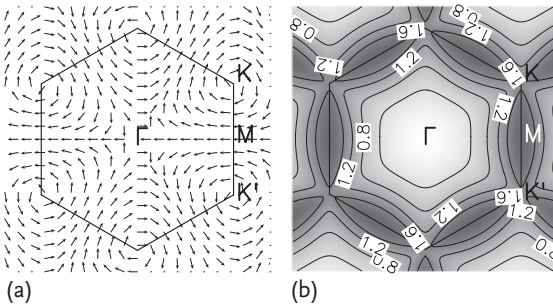
Figure 11.3 (a) The normalized electric dipole vector $\boldsymbol{D}^{cv}(\boldsymbol{k})$ is plotted as a function of $\boldsymbol{k}$ over the 2D BZ. (b) The oscillator strength in units of m_{opt} as a function of $\boldsymbol{k}$ is plotted over the 2D BZ. The separation of two adjacent contour lines is $0.4 m_{opt}$. The darker areas have a larger value for the oscillator strength [220].

This result shows that the line $p_y k_x - p_x k_y = 0$ in the 2D BZ becomes a node in the optical absorption for a given $\boldsymbol{P} = (p_x, p_y)$. In the case of graphene, however, the optical transition events take place along equi-energy contours around the K points, and we cannot see the node in Figure 11.3b. If $\boldsymbol{k}$-dependent optical absorption measurements could be carried out, this node could then be determined experimentally.

11.7
Calculation of the Electron–Phonon Interaction

The electron–phonon interaction is expressed by a modification to the tight-binding parameters by the lattice vibrations. In this section, we rewrite the wavefunction appearing in Eqs. (11.4) and (11.5) using a different notation which is suitable for calculating the electron–phonon matrix elements [222]:

$$\Psi_{a,k}(\boldsymbol{r}) = \frac{1}{\sqrt{N_u}} \sum_{s,o} C_{s,o}(a, \boldsymbol{k}) \sum_{\boldsymbol{R}_t} e^{i\boldsymbol{k}\cdot\boldsymbol{R}_t} \phi_{t,o}(\boldsymbol{r} - \boldsymbol{R}_t) , \tag{11.31}$$

where $s = A$ and B is an index denoting each of the distinct carbon atoms of graphene, and $\boldsymbol{R}_t$ is the equilibrium atom positions relative to the origin. Here $\phi_{t,o}$ denotes the atomic wave functions for the orbitals $o = 2s, 2p_x, 2p_y$, and $2p_z$ at $\boldsymbol{R}_t$, respectively. The atomic wave functions are selected as real functions.[6]

When we consider the potential energy term, V, then V can be expressed by the atomic potentials,

$$V = \sum_{\boldsymbol{R}_t} v(\boldsymbol{r} - \boldsymbol{R}_t) , \tag{11.32}$$

where v in Eq. (11.32) is the Kohn–Sham potential of a neutral pseudo-atom [263]. The matrix element for the potential energy between the initial and final states $\Psi_i = \Psi_{a,k}$ and $\Psi_f = \Psi_{a',k'}$ is

$$\langle \Psi_{a',k'}(\boldsymbol{r}) | V | \Psi_{a,k}(\boldsymbol{r}) \rangle = \frac{1}{N_u} \sum_{s',o'} \sum_{s,o} C^*_{s',o'}(a', \boldsymbol{k}') C_{s,o}(a, \boldsymbol{k})$$
$$\times \sum_{u'} \sum_{u} e^{i(-\boldsymbol{k}'\cdot\boldsymbol{R}_{u',s'} + \boldsymbol{k}\cdot\boldsymbol{R}_{u,s})} m(t', o', t, o) , \tag{11.33}$$

with the matrix element $m(t', o', t, o)$ for the atomic potential given by:

$$m(t', o', t, o) = \int \phi_{s',o'}(\boldsymbol{r} - \boldsymbol{R}_{t'}) \left\{ \sum_{\boldsymbol{R}_{t''}} v(\boldsymbol{r} - \boldsymbol{R}_{t''}) \right\} \phi_{s,o}(\boldsymbol{r} - \boldsymbol{R}_t) d\boldsymbol{r} . \tag{11.34}$$

---

6) Combining m and $-m$ states of spherical harmonic function Y_{lm}, we can get a real atomic wave function.

The atomic matrix element m comes from an integration over three centers of atoms, $\mathbf{R}_t$, $\mathbf{R}_{t'}$, and $\mathbf{R}_{t''}$. We neglect m for the cases for which all centers are different from one another. When we consider only two center integrals, m consists, respectively, of off-site and on-site matrix elements m_α and m_λ as follows:

$$m_\alpha = \int \phi_{s',o'}(\mathbf{r} - \mathbf{R}_{t'})\left\{v(\mathbf{r} - \mathbf{R}_{t'}) + v(\mathbf{r} - \mathbf{R}_t)\right\}\phi_{s,o}(\mathbf{r} - \mathbf{R}_t)d\mathbf{r} ,$$

$$m_\lambda = \int \phi_{s',o'}(\mathbf{r} - \mathbf{R}_t)\left\{\sum_{\mathbf{R}_{t'}\neq\mathbf{R}_t} v(\mathbf{r} - \mathbf{R}_{t'})\right\}\phi_{s',o}(\mathbf{r} - \mathbf{R}_t)d\mathbf{r} . \tag{11.35}$$

When we consider the amplitude of a phonon mode $\mathbf{S}(\mathbf{R}_t)$, the potential variation due to a lattice vibration is given by:

$$\delta V = \sum_{\mathbf{R}_t} v[\mathbf{r} - \mathbf{R}_t - \mathbf{S}(\mathbf{R}_t)] - v(\mathbf{r} - \mathbf{R}_t)$$

$$\approx -\sum_{\mathbf{R}_t} \nabla v(\mathbf{r} - \mathbf{R}_t)\cdot \mathbf{S}(\mathbf{R}_t) . \tag{11.36}$$

Under first-order perturbation theory, the electron–phonon matrix element is defined as [203, 222, 360–362]

$$
\begin{aligned}
M_{a,\mathbf{k}\to a',\mathbf{k}'} &= \langle \Psi_{a',\mathbf{k}'}(\mathbf{r})|\delta V|\Psi_{a,\mathbf{k}}(\mathbf{r})\rangle \\
&= -\frac{1}{N_u}\sum_{s',o'}\sum_{s,o} C_{s',o'}^*(a',\mathbf{k}')C_{s,o}(a,\mathbf{k}) \\
&\quad \times \sum_{u',u} e^{i(-\mathbf{k}'\cdot\mathbf{R}_{u',s'}+\mathbf{k}\cdot\mathbf{R}_{u,s})}\delta m(t',o',t,o) ,
\end{aligned}
\tag{11.37}
$$

where $\delta m(t',o',t,o)$ is the atomic deformation potential. Then δm can also be separated into two parts,

$$\delta m = \delta m_\alpha + \delta m_\lambda , \tag{11.38}$$

with the off-site and on-site deformation potentials δm_α and δm_λ, respectively, given by:

$$
\begin{aligned}
\delta m_\alpha &= \int \phi_{s',o'}(\mathbf{r} - \mathbf{R}_{t'})\{\nabla v(\mathbf{r} - \mathbf{R}_{t'})\cdot \mathbf{S}(\mathbf{R}_{t'}) \\
&\quad + \nabla v(\mathbf{r} - \mathbf{R}_t)\cdot \mathbf{S}(\mathbf{R}_t)\}\phi_{s,o}(\mathbf{r} - \mathbf{R}_t)d\mathbf{r} , \\
\delta m_\lambda &= \delta_{\mathbf{R}_t,\mathbf{R}_{t'}}\int \phi_{s',o'}(\mathbf{r} - \mathbf{R}_{t'})
\end{aligned}
$$

$$\times \left\{\sum_{\mathbf{R}_{t''}\neq\mathbf{R}_{t'}} \nabla v(\mathbf{r} - \mathbf{R}_{t''})\cdot \mathbf{S}(\mathbf{R}_{t''})\right\}\phi_{s',o}(\mathbf{r} - \mathbf{R}_{t'})d\mathbf{r} , \tag{11.39}$$

where the off-site and on-site atomic deformation potentials are, respectively, the corrections to off-diagonal and diagonal Hamiltonian matrix elements and both terms have the same order of magnitude [363].

When using the Slater–Koster scheme to construct tight-binding Hamiltonian matrix elements between two carbon atoms [263], the carbon $2p$ orbitals are chosen to be along or perpendicular to the bond connecting the two atoms. The four fundamental hopping and overlap integrals are (ss), $(s\sigma)$, $(\sigma\sigma)$, and $(\pi\pi)$. We follow the same procedure as was used to construct the deformation potential matrix elements $\langle\phi|\nabla v|\phi\rangle$. We introduce the matrix elements,

$$\boldsymbol{\alpha}_{p}(\tau) = \int \phi_{\mu}(\boldsymbol{r})\nabla v(\boldsymbol{r})\phi_{\nu}(\boldsymbol{r}-\boldsymbol{\tau})d\boldsymbol{r} = \alpha_{p}(\tau)\hat{I}(\alpha_{p}) \, ,$$

$$\boldsymbol{\lambda}_{p}(\tau) = \int \phi_{\mu}(\boldsymbol{r})\nabla v(\boldsymbol{r}-\boldsymbol{\tau})\phi_{\nu}(\boldsymbol{r})d\boldsymbol{r} = \lambda_{p}(\tau)\hat{I}(\lambda_{p}) \, , \qquad (11.40)$$

where $\hat{I}(\alpha_p)$ and $\hat{I}(\lambda_p)$ are unit vectors in Eq. (11.40) describing the direction of the off-site and on-site deformation potential vectors $\boldsymbol{\alpha}_p$ and $\boldsymbol{\lambda}_p$, respectively [363], and $p = \mu\nu$. The $2p$ orbital ϕ_{μ} (ϕ_{ν}) is along or perpendicular to the bond connecting the two carbon atoms and τ is the distance between the two atoms.[7] In Figure 11.4, we show the non-zero matrix elements for the (a) off-site $\boldsymbol{\alpha}_p$ and (b) on-site $\boldsymbol{\lambda}_p$ atomic deformation potentials for 2s, σ and π atomic orbitals.

In Figure 11.5, the calculated values of $\boldsymbol{\alpha}_p$ and $\boldsymbol{\lambda}_p$ are plotted as a function of interatomic distance between two carbon atoms [222]. At $r = 1.42$ Å, the bond length between a carbon atom and one of its nearest neighbors, we have $\alpha_{\pi\pi} \approx 3.2$eV/Å and $|\lambda_{\pi\pi}| \approx 7.8$eV/Å, and $|\alpha_{\pi\sigma}| \approx 24.9$eV/Å. In order to calculate the electron–phonon matrix element of Eq. (11.37) for each phonon mode, the amplitude of the
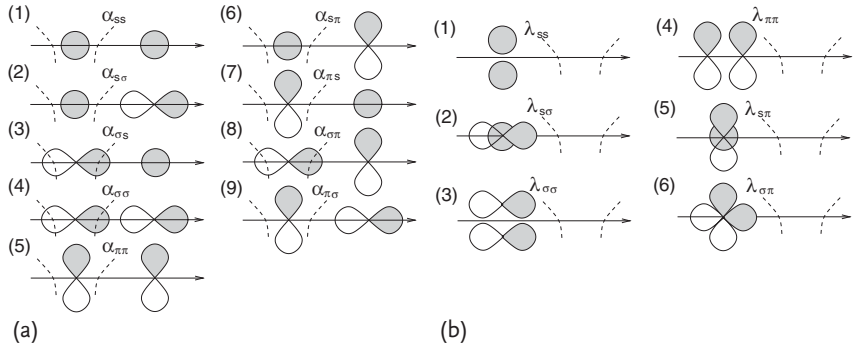

(a)

(b)

Figure 11.4 (a) The nine non-zero off-site deformation potential vectors $\boldsymbol{\alpha}_p$. The dashed curves represent the atomic potentials. (b) The six non-zero on-site deformation potential vectors $\boldsymbol{\lambda}_p$. The dashed curves represent the atomic potentials. For λ_{ss}, $\lambda_{\sigma\sigma}$, $\lambda_{\pi\pi}$ the two same orbitals are illustrated by shifting them with respect to each other [222].

7) From the matrix element $\boldsymbol{\alpha}_p$, we can deduce another matrix element,

$$\boldsymbol{\beta}_{p}(\tau) = \int \phi_{\mu}(\boldsymbol{r})\nabla v(\boldsymbol{r}-\boldsymbol{\tau})\phi_{\nu}(\boldsymbol{r}-\boldsymbol{\tau})d\boldsymbol{r}$$

$$= \int \phi_{\nu}(\boldsymbol{r})\nabla v(\boldsymbol{r})\phi_{\mu}(\boldsymbol{r}+\boldsymbol{\tau})d\boldsymbol{r} = \beta_{p}(\tau)\hat{I}(\beta_{p}). \qquad (11.41)$$

However, the integral in Eq. (11.41) can be expressed by α terms [222].
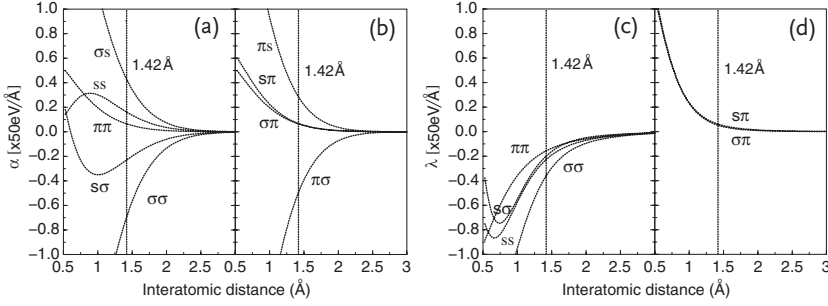
Figure 11.5 (a,b) α_p and (c,d) λ_p as a function of interatomic distance. The vertical line corresponds to 1.42 Å which is the C–C distance in graphite [222].

atomic vibration $S(R_t)$ for the phonon mode (ν, q) is calculated by

$$S(R_t) = A_\nu(q)\sqrt{\bar{n}_\nu(q)}e^\nu(R_t)e^{\pm i\omega_\nu(q)t} . \tag{11.42}$$

In Eq. (11.42) $\pm$ is for phonon emission (+) and absorption (−), respectively, and A, $\bar{n}$, e, and ω are the phonon amplitude, number, eigenvector, and frequency, respectively. At equilibrium, the phonon number in Eq. (11.42) is determined by the Bose–Einstein distribution function $n_\nu(q)$ for phonon ν,

$$n_\nu(q) = \frac{1}{e^{\hbar\omega/k_B T} - 1} . \tag{11.43}$$

Here $T = 300\,\mathrm{K}$ is the lattice temperature at room temperature and k_B is the Boltzmann constant. For phonon emission, the phonon number $\bar{n} = n + 1$ while for phonon absorption, $\bar{n} = n$. The amplitude of the zero-point phonon vibration is

$$A_\nu(q) = \sqrt{\frac{\hbar}{N_u m_C \omega_\nu(q)}} , \tag{11.44}$$

and the phonon eigenvector $e^\nu(R_t)$ is given by diagonalizing the dynamical matrix in Eq. (11.14).

11.8
Extension to Exciton States

Here we mention the procedure used to the extend the electron–photon and electron–phonon interactions into exciton–photon and exciton–phonon interactions, respectively. The detailed description is described in the original papers [186, 188] and in the exciton chapter in this book (see Chapter 10).

In the case of carbon nanotubes, a pair of photoexcited electrons and holes forms an exciton. It should be mentioned that graphene has no excitonic states. Since the exciton binding energy for nanotubes is large (on the order of 1 eV), the exciton

can exist even at room temperature. Because of the Coulomb interaction between photoexcited electrons and the holes that are left behind, the exciton wavefunction is localized in real space. When we do not consider the Coulomb interaction explicitly in the electronic structure calculation, the Bloch theorem holds for the electronic structure and thus the wavenumber k is a good quantum number in the sense that all wavefunctions and their energies are given as a function of k. The wavefunction for k is delocalized over the lattice. In order to get spatially localized wavefunctions, we mix Bloch wavefunctions with many wave vectors k with one another by the Coulomb interaction so as to minimize the excitonic energy. A mathematical picture of the Fourier transformation from real space to k space is useful. That is, when the exciton wavefunction is more localized in real space, the exciton wavefunction is more delocalized in the k space. The equation for how to mix the different k states is the so-called Bethe–Salpeter equation [186].

In Section 10.4.1 we discussed the Bethe–Salpeter equation. After solving the Bethe–Salpeter equation, we get the exciton wavefunction $|\Psi_q^n\rangle$ with a center-of-mass momentum q as

$$|\Psi_q^n\rangle = \sum_k Z_{kc,(k-q)v}^n c_{kc}^+ c_{(k-q)v}|0\rangle \,, \tag{11.45}$$

where $Z_{kc,(k-q)v}^n$ is the eigenvector of the nth $(n = 0, 1, 2, \cdots)$ state of the Bethe–Salpeter equation, $c^+ (c)$ is the creation (annihilation) operator for the electron in the conduction (valence) band with momentum $k(k - q)$, and $|0\rangle$ is the ground state. The summation on k is taken over the two-dimensional Brillouin zone (2D BZ) and $Z_{kc,(k-q)v}^n$ is localized in k space near the k point where an electron–hole pair is created.

11.8.1
Exciton–Photon Matrix Element

The exciton–photon matrix element is given by a linear combination of the electron–photon matrix element D_k at k, weighted by $Z_{kc,kv}^{n*}$

$$M_{\text{ex–op}} = \langle \Psi_0^n | H_{\text{el-op}} | 0 \rangle = \sum_k D_k Z_{kc,kv}^{n*} \,, \tag{11.46}$$

where Ψ_0^n is the exciton wavefunction with $q = 0$ center-of-mass momentum. Since the center-of-mass momentum should be conserved before and after an optical transition, it is sufficient to consider the case of $q = 0$.

In the case of a single-wall carbon nanotube, since the lattice structure is symmetric under a C_2 rotation around an axis which is perpendicular to the nanotube axis and goes over the center of a C–C bond, the C_2 exchange operation between A and B carbon atoms in the hexagonal lattice is equivalent to the exchange of k and $-k$ states. Since the exciton wavefunction of a carbon nanotube should transform as an irreducible representation of the C_2 symmetry operation, we get A_1, A_2, E, and E^* symmetry excitons (Section 10.3.1). For example, the A_1 and A_2 exciton wavefunctions which are symmetric and antisymmetric under a C_2 rotation,

respectively, are given by:

$$|\Psi_0^n(A_{1,2})\rangle = \frac{1}{\sqrt{2}} \sum_k Z_{kc,kv}^n \left(c_{kc}^+ c_{kv} \mp c_{-kc}^+ c_{-kv} \right) |0\rangle \,, \tag{11.47}$$

where k and $-k$ are located around the K and K′ points, respectively, and $-$ (+) in $\mp$ corresponds to an A_1 (A_2) exciton.[8]

When we use the relation $D_k = D_{-k}$, the excitonic-optical (ex-op) matrix elements for the A_1 and A_2 excitons are given by:

$$M_{\text{ex–op}}(A_1^n) = 0 \,,$$
$$M_{\text{ex–op}}(A_2^n) = \sqrt{2} \sum_k D_k Z_{kc,kv}^{n*} \,. \tag{11.48}$$

Equation (11.48) directly indicates that A_1 excitons are dark and only A_2 excitons are bright, which is consistent with the predictions by group theory (Section 10.3.2) [218]. Because of the spatially localized exciton wavefunction, the exciton–photon matrix elements are greatly enhanced (on the order of 100 times) compared with the corresponding electron–photon matrix elements.

11.8.2
The Exciton–Phonon Interaction

Using the creation and annihilation operators, the electron–phonon (el–ph) coupling for a phonon mode (q, ν) has the form

$$H_{\text{el–ph}} = \sum_{kq\nu} \left[M_{k,k+q}^\nu(c) c_{(k+q)c}^+ c_{kc} - M_{k,k+q}^\nu(v) c_{(k+q)v}^+ c_{kv} \right] \left(b_{q\nu} + b_{q\nu}^+ \right) \,, \tag{11.49}$$

where $M(c)$ ($M(v)$) is the el–ph matrix element for the conduction (valence) band, and $b_{q\nu}^+$ ($b_{q\nu}$) is a phonon creation (annihilation) operator for the νth phonon mode at q.

From Eq. (11.49), we obtain the exciton–phonon matrix element between the initial state $|\Psi_{q1}^{n1}\rangle$ and a final state $|\Psi_{q2}^{n2}\rangle$,

$$M_{\text{ex–ph}} = \left\langle \Psi_{q2}^{n2} \middle| H_{\text{el–ph}} \middle| \Psi_{q1}^{n1} \right\rangle$$
$$= \sum_k \left[M_{k,k+q}^\nu(c) Z_{k+q,k-q1}^{n2*} Z_{k,k-q1}^{n1} - M_{k,k+q}^\nu(v) Z_{k+q2,k}^{n2*} Z_{k+q2,k+q}^{n1} \right] \,, \tag{11.50}$$

with $q = q_2 - q_1$ accounting for momentum conservation. We can see that the exciton–phonon interaction is obtained by taking the average of the electron–phonon matrix element $M_{k,k+q}^\nu$ weighted by the exciton wavefunction.

---

8) What is confusing but correct is that "$-$" corresponds to a symmetric wavefunction and that "$+$" corresponds to an anti-symmetric wavefunction in Eq. (11.47).

Compared with the exciton–photon matrix elements, the exciton–phonon matrix elements are not enhanced significantly since the interaction area between the exciton and the phonon is decreased for the exciton wavefunction relative to that for band states.

11.9
Matrix Elements for the Resonance Raman Process

Combining all the matrix elements discussed above, we can formulate the first-order Stokes Raman intensity due to the electron–phonon interaction as

$$I_{\text{el}} = \left| \frac{1}{L} \sum_{\boldsymbol{k}} \frac{D_{\boldsymbol{k}}^2 \left[M_{\text{el–ph}}(\boldsymbol{k} \to \boldsymbol{k}, c) - M_{\text{el–ph}}(\boldsymbol{k} \to \boldsymbol{k}, v) \right]}{\left[E - E_{\text{cv}}(\boldsymbol{k}) + i\gamma_r \right] \left[E - E_{\text{cv}}(\boldsymbol{k}) - E_{\text{ph}} + i\gamma_r \right]} \right|^2 , \tag{11.51}$$

where γ_r is a broadening factor defining the resonance Raman window. The γ_r value is calculated by the life time of the photoexcited carriers [308, 364] by using the uncertainty relationship. The lifetime of the photoexcited carriers is calculated by the transition probability for emitting a phonon through the electron–phonon (or exciton–phonon) interaction. For more details see Section 11.10 on the resonance Raman window.

When we use the exciton–photon and exciton–phonon interactions which apply to single-wall carbon nanotubes, the Raman intensity for the exciton I_{ex} is given by:

$$I_{\text{ex}} = \left| \frac{1}{L} \sum_{a} \frac{M_{\text{ex–op}}(a) M_{\text{ex–ph}}(a \to b) M_{\text{ex–op}}(b)}{(E - E_a + i\gamma_r)(E - E_a - E_{\text{ph}} + i\gamma_r)} \right|^2$$

$$= \left| \frac{1}{L} \sum_{a} \frac{M_{\text{ex–op}}(a)^2 M_{\text{ex–ph}}(a \to a)}{(E - E_a + i\gamma_r)(E - E_a - E_{\text{ph}} + i\gamma_r)} \right|^2 . \tag{11.52}$$

In the second line of Eq. (11.52), we assume that the virtual state b can be approximated by the real state a. In the case of a first-order Raman process, since $\boldsymbol{q} = \boldsymbol{0}$, the matrix element of Eq. (11.50) is simplified as

$$M_{\text{ex–ph}} = \sum_{\boldsymbol{k}} \left[M_{\boldsymbol{k},\boldsymbol{k}}^{\nu}(c) - M_{\boldsymbol{k},\boldsymbol{k}}^{\nu}(v) \right] |Z_{\boldsymbol{k},\boldsymbol{k}}|^2 . \tag{11.53}$$

When we consider the second-order Raman intensity, we should consider $\boldsymbol{q} \neq \boldsymbol{0}$ phonon scattering. In this case, the exciton–phonon interaction between an A_2 exciton state and an E exciton state is important, where the E exciton state consists of an electron near the K point and a hole near the K' point and vice versa.

In this chapter, we show that we can calculate the resonance Raman spectra and the intensity combined with many calculation programs. Further, using the electron–phonon (or exciton–phonon) interaction, we can calculate the resonance window γ_r by calculating the lifetime of the photoexcited carriers (Section 9.2.1). Further, using the electron–phonon interaction for metallic energy bands, we can estimate the Raman spectral width in the case of the Kohn anomaly (Section 8.4). There

are many possibilities for using these interactions such as for coherent-phonon spectroscopy [365].

11.10
Calculating the Resonance Window Width

The width of the resonance window or the γ_r value in Eq. (11.52), of the Raman excitation profile in quantum mechanics is related by the uncertainty relation to the lifetime of the carriers. Usually, the dominant contribution to the lifetime of the carriers in the Raman spectra is in an inelastic scattering process by the emitting and absorbing phonons. In this section, we show how to calculate the carrier lifetime [360] by considering electron–phonon matrix elements [203, 222] and the Fermi Golden rule. For metallic systems (M-SWNTs), the electron–plasmon coupling contributions can shorten the lifetime (broaden the γ_r values), as discussed in [308].

The transition rate for an excited electron scattered to another electronic state can be evaluated for phonon scattering. The inverse of this transition rate is called the relaxation time τ [357, 361], which is inversely proportional to the resonance window, that is, to the γ_r value, and γ_r satisfies the uncertainty principle:

$$\gamma_r = \frac{\hbar}{\tau} . \tag{11.54}$$

The transition rate for the scattering per unit time of an excited electron from an initial state k to all possible final states k' by the νth phonon mode can be obtained by the Fermi Golden Rule [357],

$$
\begin{aligned}
\frac{1}{\tau_\nu} &= W_k^\nu \\
&= \frac{S}{8\pi M d_t} \sum_{\mu',k'} \frac{|D_\nu(k,k')|^2}{\omega_\nu(k'-k)} \left[\frac{d E(\mu',k')}{dk'}\right]^{-1} \\
&\times \left\{ \frac{\delta(\omega(k')-\omega(k)-\omega_\nu(k'-k))}{e^{\beta\hbar\omega_\nu(k'-k)}-1} \right. \\
&+ \left. \frac{\delta(\omega(k')-\omega(k)+\omega_\nu(k'-k))}{1-e^{-\beta\hbar\omega_\nu(k'-k)}} \right\} ,
\end{aligned}
\tag{11.55}
$$

where S, M, d_t, β, and μ' denote the area of the 2D graphite unit cell, the mass of a carbon atom, the diameter of a SWNT, $1/k_B T$, and the cutting line indices of the final state, respectively. Here $D_\nu(k,k')$ is a matrix for scattering an electron from k to k' by the νth phonon mode. The relaxation process is restricted to satisfying energy-momentum conservation. The two terms in brackets in Eq. (11.55) represent the absorption and emission processes, respectively, of the νth phonon mode with energy $\hbar\omega_\nu(k'-k)$.

With this result for the case of S-SWNTs, we can get calculated γ_r values in agreement with experiment, by just considering the electron–phonon coupling mod-

el [308]. We can see that the γ_r value shows a strong dependence on chirality and diameter for S-SWNTs. However, the γ_r value calculation for M-SWNTs needs an additional contribution, such as might come from the electron–plasmon interaction, because the calculated γ_r value that considers only the electron–phonon interaction is not consistent with experimental results, that is, calculations give a considerably underestimated γ_r value compared with experiment. Here new physics, such as the interaction between the excited electron in the conduction band and the plasmon associated with two linear energy bands have to be considered. In order to apply a detailed electron–plasmon effect to the γ_r value calculation, more in-depth research has to be done.

11.11
Summary

The diameter distribution of a pristine SWNT sample can be determined by HRTEM and this result was compared with the RBM RRS map for the same sample. Under the assumption of an equal distribution of chiral angles, the RRS RBM cross-section of the SWNTs was determined and it was seen that it can be well represented by a simple empirical formula. The RBM intensity can then be used in the inverse process to yield the sample's diameter distribution.

The observed (n, m) dependent matrix elements and resonance window widths were then addressed theoretically, based on a tight-binding model for electrons and phonons in graphene and carbon nanotubes. Excitons are also addressed. The calculational methods are important not only for explaining the RBM results, but also for interpreting the Raman spectra of sp^2 carbon systems more generally.

Problems

[11-1] Consider two π orbitals on two carbon atoms. When we assume that the nearest neighbor tight-binding parameters for the Hamiltonian and overlap matrices are γ_0 and s_0, obtain the eigenenergies for the bonding and antibonding orbitals.

[11-2] Obtain a tight-binding Hamiltonian matrix for single-layer graphene. Consider two cases: (1) consider only the nearest-neighbor interaction and (2) consider up to the third nearest-neighbor interaction.

[11-3] In the previous problem, also consider the overlap matrix elements.

[11-4] Obtain a tight-binding Hamiltonian matrix for bilayer graphene. Consider the two cases: (1) consider only the γ_1 band parameter and (2) consider the γ_1, γ_3 and γ_4 band parameters. In the case of bilayer graphene, we also need to consider the energy E_0^e.

[11-5] Obtain a tight-binding Hamiltonian matrix for trilayer graphene in which we consider band parameters from γ_0 to γ_5. In the case of trilayer graphene, we also need to consider the energy Δ which differentiates A and B carbon sites from one another.

[11-6] For the case of bilayer graphene, obtain the electronic energy dispersion numerically. What is the role of γ_3 and γ_4 in the energy dispersion near the K point?

[11-7] In the case of single-layer graphene, show explicitly the relationship between the force constant sum rule for ϕ_{ti} and that for ϕ_{to}.

[11-8] Show that the in-plane and out-of-plane phonon modes are decoupled in the dynamical matrix when we use the force constant models.

[11-9] In the case of phonons around the K point, we can consider zone folding in which the K point phonon modes are folded into the Γ point if we consider a super-cell structure. What kind of super-cell structure is needed for obtaining the zone folding for the K point phonon mode?

[11-10] Discuss the selection rule between the atomic orbitals which are specified by ℓ, m, n atomic quantum numbers. Show the optically allowed states for 2p orbitals as an initial state.

[11-11] Show that the relationship between the electric field E for light in vacuum and the vector potential A is given by $E = i\omega A$.

[11-12] Using the Poynting vector, $I = EB/\mu_0 = E^2/(\mu_0 c)$, obtain Eq. (11.21).

[11-13] Using the simplest tight-binding Hamiltonian, obtain the wavefunction coefficients in Eq. (11.27) around $K = (0, -4\pi/(3a))$.

[11-14] Obtain the wavefunction coefficient around $K' = (0, 4\pi/(3a))$, and the dipole vector $D^{cv}(K' + k) = [3m_{opt}/2k](-k_y, k_x, 0)$. Explain that the rotational directions of $D^{cv}(k)$ around the K and K' points are opposite to each other.

[11-15] When the crystal potential (Eq. (11.32)) is periodic, show that the matrix elements of Eq. (11.33) have non-zero values only for $k = k'$.

[11-16] In Figure 11.6, another set of off-site deformation potential vectors $\boldsymbol{\beta}_p$ are shown. By comparing $\boldsymbol{\beta}_p$ with $\boldsymbol{\alpha}_p$ in Figure 11.4, show that the following relationships between $\boldsymbol{\beta}_p$ and $\boldsymbol{\alpha}_p$ hold:

$$\begin{aligned}
\boldsymbol{\beta}_{ss} &= -\boldsymbol{\alpha}_{ss}, \quad \boldsymbol{\beta}_{s\sigma} = \boldsymbol{\alpha}_{\sigma s}, \\
\boldsymbol{\beta}_{\sigma s} &= \boldsymbol{\alpha}_{s\sigma}, \quad \boldsymbol{\beta}_{\sigma\sigma} = -\boldsymbol{\alpha}_{\sigma\sigma}, \\
\boldsymbol{\beta}_{\pi\pi} &= -\boldsymbol{\alpha}_{\pi\pi}, \quad \boldsymbol{\beta}_{s\pi} = \boldsymbol{\alpha}_{\pi s}, \\
\boldsymbol{\beta}_{\pi s} &= \boldsymbol{\alpha}_{s\pi}, \quad \boldsymbol{\beta}_{\sigma\pi} = -\boldsymbol{\alpha}_{\pi\sigma}, \\
\boldsymbol{\beta}_{\pi\sigma} &= -\boldsymbol{\alpha}_{\sigma\pi}.
\end{aligned} \tag{11.56}$$
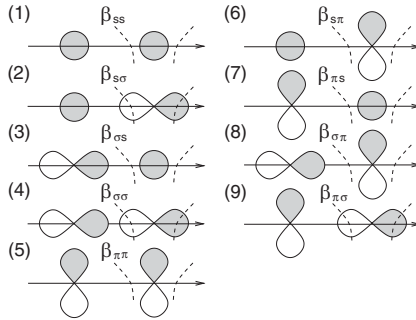
Figure 11.6 The nine non-zero off-site deformation potential vectors $\boldsymbol{\beta}_{\mathrm{p}}$. The dashed curves represent the atomic potential.

[11-17] Consider the *E* exciton wavefunction and show that *E* exciton states do not contribute to an optical absorption (or emission).

[11-18] When we consider the phonon emission from a photoexcited carrier by the electron–phonon interaction, show by illustrating in a figure that there are 24 possible final states in graphene which satisfy energy-momentum conservation.

[11-19] In Eq. (11.49), we consider the scattering of a hole in the second term. Explain why the minus sign in $-M^{\nu}_{k,k+q}(\nu)$ appears.

[11-20] When the excitation energy is not resonant with the energy separation between an occupied and an unoccupied state, time-dependent perturbation theory tells us that the optical transition probabilities to possible real states are non-zero. Then we can consider a virtual state whose energy is determined by the energy of the light. Show that the virtual state can be expressed by a linear combination of the real states. Especially when the virtual state position is close to a real state, show that the coefficient of the real state is then close to unity and thus we can approximate the virtual state by the real state.